Received June 5, 2019, accepted July 12, 2019, date of publication July 25, 2019, date of current version August 12, 2019.

Digital Object Identifier 10.1109/ACCESS.2019.2930755

Amorphous MgInO Ultraviolet Solar-Blind Photodetectors

KUAN-YU CHEN[1,2], HOANG-TUAN VU[3], CHIH-CHIANG YANG[2], CHING-CHIEN HSU[1], AND YAN-KUIN SU[1,2], (Life Fellow, IEEE)

[1]Department of Electrical Engineering, Institute of Microelectronics, National Cheng Kung University, Tainan 701, Taiwan
[2]Green Energy Technology Research Center, Department of Electrical Engineering, Kun Shan University, Tainan 710, Taiwan
[3]Research and Development Department, RiTdisplay Corporation, Hsinchu Industrial Park, Hukou 303, Taiwan

Corresponding authors: Chih-Chiang Yang (298r.yang@gmail.com) and Yan-Kuin Su (yksu@mail.ncku.edu.tw)

This work was supported in part by the Ministry of Science and Technology of Taiwan, ROC, under Grant MOST107-2221-E-006 -185 -MY3 and Grant 108-2221-E-006-201-MY3, and in part by the Green Energy Technology Research Center, Department of Electrical Engineering, Kun Shan University, Tainan, Taiwan through The Featured Areas Research Center Program within the framework of the Higher Education Sprout Project by the Ministry of Education (MOE) in Taiwan.

ABSTRACT The magnesium oxide is one of the promising candidate's materials that can act as solar blind photodetectors. However, the intrinsically low thermal conductivity of MgO, which is restrict the application in electric device. The magnesium oxide exhibits the poor conductivity which could improved by doing method. This paper fabricated magnesium indium oxide (MgInO) solar-blind photodetectors by doping indium oxide with magnesium oxide through co-sputtering deposition method. The photodetector comprises a bottom glass substrate, an MgInO thin film, and an interdigitated gold electrode to complete the metal–semiconductor–metal structure of the solar-blind photodetector. The experimental results indicate that the photo-to-dark-current ratio is 1.4×10^4, and the responsivity is 1.47 A/W when a reverse bias voltage of 2 V is applied. Furthermore, the noise equivalent power and detectivity are 7.77×10^{-11} W and 1.75×10^{11} cm H $^{0.5}$ W^{-1} with a 2 V bias voltage, respectively.

INDEX TERMS MgInO, photodetectors, solar blind.

I. INTRODUCTION

Ultraviolet (UV) photodetectors have numerous important applications. Photodetectors operating in the solar-blind region caused by their low natural background permit several applications, such as ozone monitoring, microbial decontamination processing, UV phototherapy, and spectrophotometry analysis. UV light can be divided into solar (wavelengths below 290 nm) and visible (wavelengths below 400 nm) blinds; the UV wavelength working region of the fabricated solar-blind detector is located at UV-C (280–100 nm) [1]. These application examples must use UV light at UV-C, so a short-wavelength UV light detector is probable.

Wide-bandgap materials can have a large energy band depending on the cutoff wavelength, so they are suitable for detecting UV light. Common wide-bandgap materials, such as ZnO, TiO_2, SnO_2, gallium oxide (Ga_2O_3) and [2]–[6], were reported in previous articles. Ga_2O_3 exhibits high-transparency and high-breakdown electrical field with a band gap of 4.9 eV, which is naturally suitable for solar-blind detection. Ga_2O_3 has been used in photodetector, power device, and resistive element [7]. However, Ga_2O_3 exhibits poor conductivity caused by the large energy band gap, which can increase the conductivity by the method for enhanced device performance [8]. Solar blind is increasingly used in the solar-blind region to tune the energy bandgap through doping method, such as the MgZnO, ZnGaO, and AGO [9]–[11] material systems.

MgO possesses low electrical conductivity but high thermal conductivity. This low electrical conductivity can be solved by doping indium oxide (In_2O_3) with MgO. In_2O_3 is an n-type semiconductor material, has high conductivity, and has a direct wide energy gap. In_2O_3 has a bandgap of 3.75 eV in the visible-blind region, which is suitable for a visible-blind photodetector. By contrast, the energy band of MgO is approximately 7.7 eV. The energy gap and conductivity of MgO can be modulated by doping In_2O_3 with components used in the solar-blind region. Doping can increase the electron concentration to improve the electrical

The associate editor coordinating the review of this manuscript and approving it for publication was Fabio Massaro.

characteristics and reliability of components [12]. Previous studies indicated that doping In_2O_3 with another metal, such as ZnO, Zr, Al, and Ga [13]–[16], can enhance electrical properties and stability and be used in various semiconductor components.

Wenckstern *et al.* [17] introduced $(In_xGa_{1-x})_2O_3$ thin film with variation of the indium content for application in solar-blind region. Zheng *et al.* [18] introduced $Mg_{0.49}Zn_{0.51}$ O-based metal -semiconductor-metal solar blind photodetectors on lattice matched ZnO substrates by using cosputtering method. Liu *et al.* [19] reported Zn_2GeO_4 and $In_2Ge_2O_7$ nanowire mats ultraviolet photodetectors on rigid and flexible substrate by using a chemical vapor deposition (CVD) method. To date, doping In_2O_3 with MgO has not been reported for use in UV photodetector, so it is worth exploring.

Photodetectors can be classified by structures, such as p-n, p-i-n, avalanche, and metal–semiconductor–metal (MSM) photodetectors [20]–[24]. We build upon the MSM structure owing to its easy fabrication and low capacitance. In the present work, MgO-doped In_2O_3 MSM-structured solar-blind photodetectors are fabricated by co-sputtering, and the I-V characteristic, responsivity, and noise properties are reported.

II. DEVICE FAVRICATION AND CHARACTERIZATION

To fabricate a UV photodetector, a glass substrate was cleaned by using acetone, isopropanol, and deionized water. This process was repeated thrice to remove the particles or grease from the glass. First, the magnesium indium oxide (MgInO) film was deposited on the glass substrate by co-sputtering using In_2O_3 and MgO targets. The In_2O_3 and MgO powers were 30 and 100 W at 1×10^{-6} Torr, respectively. The flow rate of Ar was set at 50 sccm, trace oxygen was added, and the growth pressure was 5 mTorr. After MgInO thin film deposition, the film was annealed in 50 sccm Ar flow at 300 °C for 1 h. An Au layer was deposited into MgInO thin films through an interdigitated shadow mask by electron beam evaporation. The schematic diagram is shown in Fig 1. The total optical area was $0.18 mm^2$. Finally, components were produced. The thickness of the electrode layer and MgInO thin film layer was 100 nm. All parameters were analyzed using an Agilent B1500A semiconductor device analyzer. For the UV light source, the 150 W Xenon lamp was used in our experiments. All measurements were conducted at room temperature in dark room.

III. RESULTS AND DISCUSSION

Fig. 2 shows the X-ray diffraction (XRD) diagram of MgInO thin film. No diffraction peaks can be found. The result demonstrates that the MgInO thin film is amorphous phase. Fig.3. illustrates the energy bandgap of In_2O_3, MgInO, and MgO. A Tauc plot was used to determine the optical energy bandgap, as shown in the following equation:

$$(\alpha h\nu)^2 = A(h\nu - E_g) \tag{1}$$

where α is the absorption coefficient, $h\upsilon$ denotes the photoenergy, A is a constant and Eg represents the energy bandgap. The optical energy bandgaps of In_2O_3 and MgInO were approximately 3.7 and 4.46 eV, respectively. The bandgap of MgO cannot be measured; the theoretical value of MgO was 7.7 eV [25]. We prepared the MgInO film, which confirmed that the incorporation of In_2O_3 into MgO can adjust the energy gap. Also, it is worth noting that the composition of the In in MgInO were 9.98 at%.

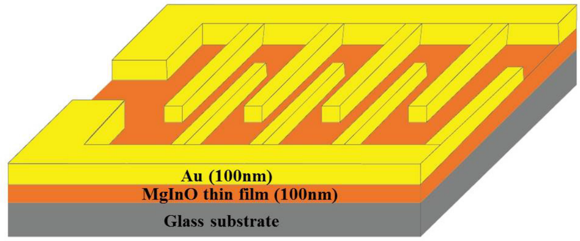

FIGURE 1. Schematic of MgInO PDs.

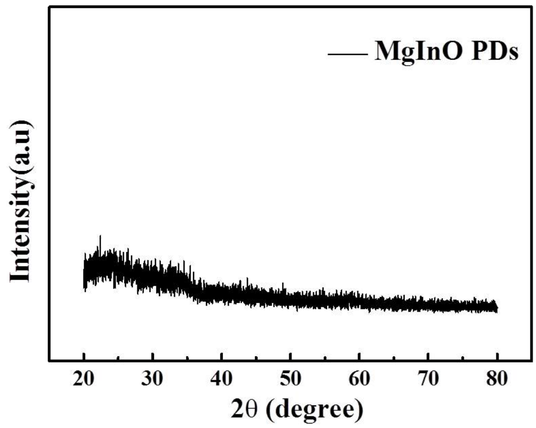

FIGURE 2. XRD diagrams of MgInO PDs.

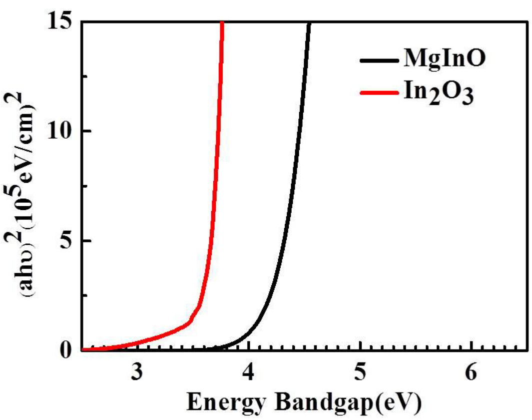

FIGURE 3. Absorption coefficient spectra of MgInO thin films.

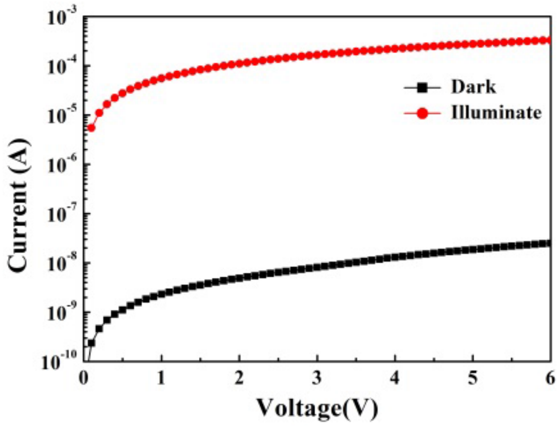

FIGURE 4. I-V characteristics of MgInO PDs.

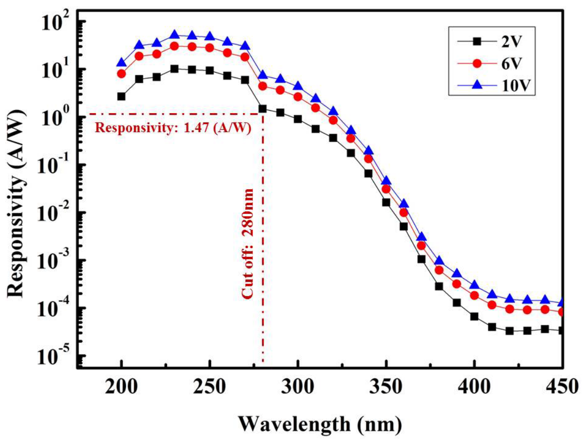

FIGURE 5. Responsivity of MgInO PDs with various applied bias voltages.

Furthermore, the cutoff wavelength of the film was in the solar-blind UV spectral region.

The I-V characteristics of MgInO PDs were measured under dark and UV illumination ($\lambda = 280$ nm) conditions as shown in Fig. 4. With an applied bias voltage of 6 V, the photo current was 3.3×10^{-4} A, and the dark current was 2.5×10^{-8} A. Therefore, the photo-to-dark-current ratio (I_{ph}/I_{dark}) was 1.32×10^4. The amplified current was significantly observed under UV illumination. The responsivity of the device was measured by applying various bias voltages at 200–450 nm wavelength range as shown in Fig. 5:

$$R = \frac{I_{light} - I_{dark}}{P_{opt}} = \frac{I_{ph}}{P_{opt}} \tag{2}$$

where I_{light} is the photo current, I_{dark} indicates the dark current, and P_{opt} represents the incident optical power. The responsivity of MgInO PDs with an applied bias voltage of 2 V was 1.47 A/W at the wavelength of 280 nm. The MgInO PD response in the 290–350 nm wavelength range indicated that the photoenergy was lower than the bandgap energy that still has a response, which means the photo generated carriers assisted with defect states. The defect can

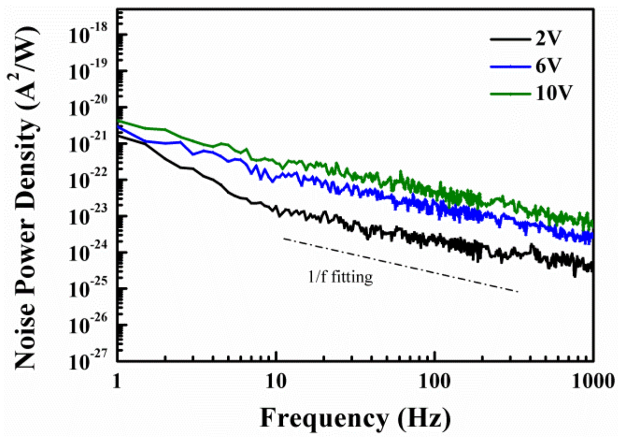

FIGURE 6. Noise power densities of MgInO PDs under various voltages.

be trap states and band tail states by structure defect, which especially in the amorphous metal oxide system [26]. The UV-to-visible rejection ratio was defined as the responsivity measured at 280 nm divided by the responsivity measured at 450 nm.

Based on the definition, the UV-to-visible rejection ratio was 4.37×10^4 at an applied bias voltage of 2 V. A high UV-to-visible rejection ratio by four orders of magnitudes, such as MgInO PDs, is potentially used for solar-blind photodetector. Fig. 6. shows the noise power spectra of MgInO PDs at various bias voltages and a measurement frequency of 1–1000 Hz in the dark region. When a high voltage was applied, the noise power was increased. Photodetectors have four types of noise: shot, generation–recombination, thermal, and flicker noises (1/f). Flicker is a low-frequency noise that affects the low-frequency range. Flicker noise caused by material defects or the imperfection of the fabrication process leads to mobility fluctuation caused by lattice and impurity scattering [27]. Generally, the noise spectral density power can use a Hooge-type equation:

$$S_n(f) = S_0\left(\frac{I_d^{\beta}}{f^{\alpha}}\right), \tag{3}$$

where S_o is a bias-independent constant, I_d denotes the dark current of the device, and α and β represent the fitting parameters. This measurement shows that the main noise of MgInO PDs is flicker noise. To measure the noise equivalent power (NEP) and normalized detectivity (D∗), the total noise current power of the PDs can be determined through the following equation:

$$\begin{aligned} \langle in \rangle^2 &= \int_0^B S_n(f)\,df \\ &= \int_0^1 S_n(1)\,df \\ &= S_0[\ln(B) + 1] \end{aligned} \tag{4}$$

which is calculated by integrating Sn(f) for a given bandwidth (B). The NEP can be obtained through the following

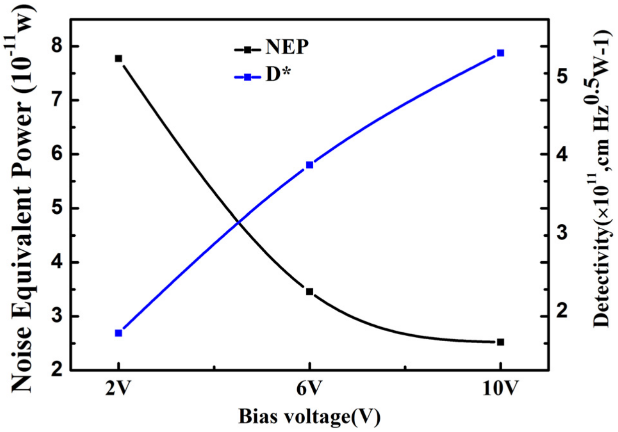

FIGURE 7. NEP and D* of MgInO PDs under various bias voltages.

equation:

$$NEP = \frac{\sqrt{\langle in \rangle}^2}{\mathrm{R}} \tag{5}$$

where R is the responsivity of PDs. The normalized detectivity can be expressed by:

$$D^* = \frac{\sqrt{A}\sqrt{B}}{NEP} \tag{6}$$

where A indicates the area of PDs, which is 0.18 cm^2, and B represents the bandwidth, which is 1000 Hz. Fig. 7. shows the calculated NEP and D* with various applied bias voltages. The NEP of MgInO PDs was 7.77×10^{-11} W with an applied bias voltage of 2 V. After calculation, the D* of MgInO PDs was 1.75×10^{11} cm $Hz^{0.5}$ W^{-1} under an applied bias voltage of 2V. The photo current generation mechanism of a semiconductor is including electro-hole generation from valence-band to conduction band and defect conduction ban transition when under the UV illumination. On the other hand, the electrons recombine with holes through the recombination centers or band-to-band annihilation process during the illuminate is turn off [28]. As regard, the MgInO MSM PD exhibited the schottky behavior can be explained as follows Guo *et al.* [5]. The fewer oxygen vacancies imply the depletion region is thick in the dark, which hinders to charge transportation In this situation, the charge carrier mainly determined by the thermionic emission.

To summarize, Table 1 shows the performance of MgInO PDs compared with that of different material systems in other studies, from the cutoff wavelength, which can be calculated by Eg (eV) = 1240/λ. The MgO can tunable by alloying with In_2O_3 as promising candidates for solar-blind detection; thus, this material system can be applied in field-emission, transistors, or fabrication on flexible substrate [29]–[32]. Meanwhile, Guo et al. reported β-Ga_2O_3-based solar-blind photodetectors based on heterojunction structure and pn junction structure to improve the photoconductive type photodetector performance because of the persistent photo-conductivity effect [33]–[35]. Therefore, the MgInO photodetector can consider above structure to fabricate a zero-power consumption solar-blind photodetector.

TABLE 1. Performance of MgInO PDs Compared With Other Solar-Blind Photodetectors.

Sample	Applied bias (V)	Responsivity (A/W)	cut wavelength (nm)	Fabrication method	Ref
MgInO	2	1.47	280	RF sputter	This work
GaZTO	10	0.091	280	RF sputter	[36]
Ga_2O_3	5	0.903	250	Pulsed laser deposition	[37]
$Mg_xZn_{1-x}O$	3	0.31	284	RF sputter	[38]
Al_2O_3-alloyed Ga_2O_3	5	0.12	250	RF sputter	[39]

IV. CONCLUSION

MgInO MSM solar-blind photodetectors were fabricated on glass by co-sputtering using MgO and In_2O_3 targets at room temperature. The optical bandgap energy of MgInO was 4.46 eV, and the cut-off wavelength was approximately 280 nm. The responsivity increased with the measured voltage. The measured voltage increased with the NEP and D*. Furthermore, the responsivity of MgInO PDs with an applied bias voltage of 2 V was 1.47 A/W. The UV-to-visible rejection ratio was 4.37×10^4 at an applied bias voltage of 2 V. The noise equivalent power of 7.77×10^{-11} W and the detectivity of 1.75×10^{11} cm $Hz^{0.5}$ W^{-1} were observed.

REFERENCES

[1] H. Chen, K. Liu, L. Hu, A. A. Al-Ghamdi, and X. Fang, "New concept ultraviolet photodetectors," *Mater. Today*, vol. 18, no. 9, pp. 493–502, Nov. 2015.

[2] S. I. Inamdar and K. Y. Rajpure, "High-performance metal–semiconductor–metal UV photodetector based on spray deposited ZnO thin films," *J. Alloys Compounds*, vol. 595, pp. 55–59, May 2014.

[3] W. J. Wang, C. X. Shan, H. Zhu, F. Y. Ma, D. Z. Shen, X. W. Fan, and K. L. Choy, "Metal–insulator–semiconductor–insulator–metal structured titanium dioxide ultraviolet photodetector," *J. Phys. D, Appl. Phys.*, vol. 43, no. 4, Jan. 2010, Art. no. 045102.

[4] J.-M. Wu and C.-H. Kuo, "Ultraviolet photodetectors made from SnO_2 nanowires," *Thin Solid Films*, vol. 517, no. 14, pp. 3870–3873, May 2009.

[5] D. Y. Guo, Z. P. Wu, Y. H. An, X. C. Guo, X. L. Chu, C. L. Sun, L. H. Li, P. G. Li, and W. H. Tang, "Oxygen vacancy tuned Ohmic-Schottky conversion for enhanced performance in β-Ga_2O_3 solar-blind ultraviolet photodetectors," *Appl. Phys. Lett.*, vol. 105, no. 2, Jul. 2014, Art. no. 023507.

[6] D. Guo, Y. Su, H. Shi, P. Li, N. Zhao, J. Ye, S. Wang, A. Liu, Z. Chen, C. Li, W. Tang, and "Self-powered ultraviolet photodetector with superhigh photoresponsivity (3.05 A/W) based on the GaN/Sn:Ga_2O_3 pn junction," *ACS Nano*, vol. 28, pp. 12827–12835, Nov. 2018.

[7] S. J. Pearton, J. Yang, P. H. Cary, F. Ren, J. Kim, M. J. Tadjer, and M. A. Mastro, "A review of Ga_2O_3 materials, processing, and devices," *Appl. Phys. Rev.*, vol. 5, no. 1, Jan. 2018, Art. no. 011301.

[8] W. Mi, X. Du, C. Luan, H. Xiao, and J. Ma, "Electrical and optical characterizations of β-Ga_2O_3: Sn films deposited on MgO (110) substrate by MOCVD," *RSC Adv.*, vol. 4, no. 58, pp. 30579–30583, 2014.

[9] L. K. Wang, Z. G. Ju, C. X. Shan, J. Zheng, D. Z. Shen, B. Yao, D. X. Zhao, Z. Z. Zhang, B. H. Li, and J. Y. Zhang, "MgZnO metal–semiconductor–metal structured solar-blind photodetector with fast response," *Solid State Commun.*, vol. 149, nos. 45–46, pp. 2021–2023, Dec. 2009.
[10] F. Alema, F. Alema, B. Hertog, O. Ledyaev, D. Volovik, G. Thoma, R. Miller, A. Osinsky, P. Mukhopadhyay, S. Bakhshi, H. Ali, and W. V. Schoenfeld, "Solar blind photodetector based on epitaxial zinc doped Ga_2O_3 thin film," *Physica Status Solidi A-Appl. Mater. Sci.*, vol. 214, no. 5, May 2017, Art. no. 1600688.
[11] S.-H. Yuan, C.-C. Wang, S.-Y. Huang, and D.-S. Wuu, "Improved responsivity drop from 250 to 200 nm in sputtered gallium oxide photodetectors by incorporating trace aluminum," *IEEE Electron Device Lett.*, vol. 39, no. 2, pp. 220–223, Feb. 2018.
[12] K. Xu, "Monolithically integrated Si gate-controlled light-emitting device: Science and properties," *J. Opt.*, vol. 20, no. 2, Jan. 2018, Art. no. 024014.
[13] M. N. Fujii, Y. Ishikawa, R. Ishihara, J. van der Cingel, M. R. T. Mofrad, J. P. S. Bermundo, E. Kawashima, S. Tomai, K. Yano, and Y. Uraoka, "Nano-crystallization in ZnO-doped In_2O_3 thin films via excimer laser annealing for thin-film transistors," *AIP Adv.*, vol. 6, no. 6, 2016, Art. no. 065216.
[14] Q. Yang, Y. Wang, J. Liu, J. Liu, Y. Gao, P. Sun, Z. Jie, T. Zhang, Y. Wang, and G. Lu, "Enhanced sensing response towards NO2 based on ordered mesoporous Zr-doped In_2O_3 with low operating temperature," *Sens. Actuators B, Chem.*, vol. 241, pp. 806–813, Mar. 2017.
[15] J. Shen, F. Li, B. Yin, L. Sun, C. Chen, S. Wen, Y. Chen, and S. Ruan, "Enhanced ethyl acetate sensing performance of Al-doped In_2O_3 microcubes," *Sens. Actuators B, Chem.*, vol. 253, pp. 461–469, Dec. 2017.
[16] J. Sheng, E. J. Park, B. Shong, and J. S. Park, "Atomic layer deposition of an indium gallium oxide thin film for thin-film transistor applications," *ACS Appl Mater Interfaces*, vol. 9, no. 28, pp. 23934–23940, Jul. 2017.
[17] H. von Wenckstern, D. Splith, M. Purfürst, Z. Zhang, C. Kranert, S. Müller, M. Lorenz, and M. Grundmann, "Structural and optical properties of $(In,Ga)_2O_3$ thin films and characteristics of Schottky contacts thereon," *Semicond. Sci. Technol.*, vol. 30, no. 2, Jan. 2015, Art. no. 024005.
[18] Q. Zheng, F. Huang, K. Ding, J. Huang, D. Chen, Z. Zhan, and Z. Lin, "MgZnO-based metal-semiconductor-metal solar-blind photodetectors on ZnO substrates," *Appl. Phys. Lett.*, vol. 98, no. 22, May 2011, Art. no. 221112.
[19] Z. Liu, H. Huang, B. Liang, X. Wang, Z. Wang, D. Chen, and G. Shen, "Zn_2GeO_4 and $In_2Ge_2O_7$ nanowire mats based ultraviolet photodetectors on rigid and flexible substrates," *Opt Express*, vol. 20, no. 3, pp. 2982–2991, Jan. 2012.
[20] S. W. Lee, S.-H. Cha, K.-J. Choi, B.-H. Kang, J.-S. Lee, S.-W. Kim, J.-S. Kim, H.-M. Jeong, S.-A. Gopalan, D.-H. Kwon, and S.-W. Kang, "Low dark-current, high current-gain of PVK/ZnO nanoparticles composite-based UV photodetector by PN-heterojunction control," *Sensors*, vol. 16, no. 1, p. 74, Jan. 2016.
[21] J. Werner, M. Oehme, M. Schmid, M. Kaschel, A. Schirmer, E. Kasper, and J. Schulze, "Germanium-tin p-i-n photodetectors integrated on silicon grown by molecular beam epitaxy," *Appl. Phys. Lett.*, vol. 98, no. 6, Feb. 2011, Art. no. 061108.
[22] J. Yu, C. X. Shan, X. M. Huang, X. W. Zhang, S. P. Wang, and D. Z. Shen, "ZnO-based ultraviolet avalanche photodetectors," *J. Phys. D, Appl. Phys.*, vol. 46, no. 30, Jul. 2013, Art. no. 305105.
[23] M. Morschbach, M. Oehme, and E. Kasper, "Visible light emission by a reverse-biased integrated silicon diode," *IEEE Trans. Electron Devices*, vol. 54, no. 5, pp. 1091–1094, May 2007.
[24] A. S. Pratiyush, S. Krishnamoorthy, S. V. Solanke, Z. Xia, R. Muralidharan, S. Rajan, and D. N. Nath, "High responsivity in molecular beam epitaxy grown β-Ga_2O_3 metal semiconductor metal solar blind deep-UV photodetector," *Appl. Phys. Lett.*, vol. 110, no. 22, 2017, Art. no. 221107.
[25] D. M. Roessler and W. C. Walker, "Spin-orbit splitting of the τ exciton in MgO," *Phys. Rev. Lett.*, vol. 17, no. 6, pp. 319–320, Aug. 1966.
[26] L. S. Feng, G. Yu, X. Li, J. Zhang, Z. Ye, and J. Lu, "Solution processed amorphous ZnSnO thin-film phototransistors," *IEEE Trans. Electron Devices*, vol. 64, no. 1, pp. 206–210, Jan. 2017.
[27] F. N. Hooge, "1/f noise sources," *IEEE Trans. Electron Devices*, vol. 41, no. 11, pp. 1926–1935, Nov. 1994.
[28] D. Guo, Z. Wu, P. Li, Y. An, H. Liu, X. Guo, H. Yan, G. Wang, C. Sun, L. Li, and W. Tang, "Fabrication of β-Ga_2O_3 thin films and solar-blind photodetectors by laser MBE technology," *Opt. Mater. Express*, vol. 4, no. 5, pp. 1067–1076, 2014.
[29] C.-H. Hsiao, C.-S. Huang, S.-J. Young, S.-J. Chang, J.-J. Guo, C.-W. Liu, and T.-Y. Yang, "Field-emission and photoelectrical characteristics of Ga–ZnO nanorods photodetector," *IEEE Trans. Electron Devices*, vol. 60, no. 6, pp. 1905–1910, Jun. 2013.
[30] Y. H. Liu, S.-J. Young, L. W. Ji, T. H. Meen, C. H. Hsiao, C. S. Huang, and S.-J. Chang, "UV enhanced field emission performance of Mg-doped ZnO nanorods," *IEEE Trans. Electron Devices*, vol. 61, no. 5, pp. 1541–1545, May 2014.
[31] S. M. Peng, Y.-K. Su, L.-W. Ji, S.-J. Young, C.-N. Tsai, W.-C. Chao, Z.-S. Chen, and C.-Z. Wu, "Semitransparent field-effect transistors based on ZnO nanowire networks," *IEEE Electron Device Lett.*, vol. 32, no. 4, pp. 533–535, Apr. 2011.
[32] T.-P. Chen, S.-J. Young, S.-J. Chang, C.-H. Hsiao, and Y.-J. Hsu, "Bending effects of ZnO nanorod metal–semiconductor–metal photodetectors on flexible polyimide substrate," *Nanosc. Res. Lett.*, vol. 7, no. 1, p. 214, Apr. 2012.
[33] D. Y. Guo, H. Z. Shi, Y. P. Qian, M. Lv, P. G. Li, Y. L. Su, Q. Liu, K. Chen, S. L. Wang, C. Cui, C. R. Li, and W. H. Tang, "Fabrication of β-Ga_2O_3/ZnO heterojunction for solar-blind deep ultraviolet photodetection," *Semicond. Sci. Technol.*, vol. 32, no. 3, pp. 1067–1076, Oct. 2017.
[34] D. Guo, H. L. P. Li, Z. Wu, S. Wang, C. Cui, C. Li, and W. Tang, "Zero-power-consumption solar-blind photodetector based on β-Ga2O3/NSTO heterojunction," *ACS Appl. Mater. Inter.*, vol. 9, no. 2, pp. 1619–1628, Jan. 2017.
[35] X. Li, W. Liu, P. Li, J. Song, Y. An, J. Shen, S. Wang, and D. Guo, "A self-powered nano-photodetector based on PFH/ZnO nanorods organic/inorganic heterojunction," *Results Phys.*, vol. 8, pp. 468–472, Mar. 2018.
[36] J.-C. Syu, M.-H. Hsu, S.-P. Chang, S.-J. Chang, and L. Lu, "Effect of oxygen vacancy ratio on a GaZTO solar-blind photodetector," *Coatings*, vol. 8, no. 9, p. 293, Aug. 2018.
[37] F.-P. Yu, S.-L. Ou, and D.-S. Wuu, "Pulsed laser deposition of gallium oxide films for high performance solar-blind photodetectors," *Opt. Mater. Express*, vol. 5, no. 5, pp. 1240–1249, 2015.
[38] D. Jiang, C. Tian, G. Yang, J. Qin, Q. Liang, J. Zhao, J. Hou, and S. Gao, "$Mg_xZn_{1-x}O$ solar-blind photodetectors fabricated by RF magnetron sputtering with combinatorial targets," *Mater. Res. Bull.*, vol. 67, pp. 158–161, Jul. 2015.
[39] H.-Y. Lee, J.-T. Liu, and C.-T. Lee, "Modulated Al_2O_3-alloyed Ga_2O_3 materials and deep ultraviolet photodetectors," *IEEE Photon. Technol. Lett.*, vol. 30, no. 6, pp. 549–552, Mar. 15, 2018.